SMALL SHELLY FOSSIL PRESERVATION AND THE ROLE OF EARLY DIAGENETIC REDOX IN THE EARLY TRIASSIC

SARA B. PRUSS[1,*], NICHOLAS J. TOSCA[2], COURCELLE STARK[1]

[1]*Department of Geosciences, Smith College, Northampton, MA 01063, USA,*

spruss@smith.edu, *cstark@smith.edu*

[2]*Department of Earth Sciences, Oxford University, Oxford, OX1 3AN, UK,*

nick.tosca@earth.ox.ac.uk

*Corresponding author

Keywords: Lower Triassic, Virgin Limestone, diagenesis, taphonomy, end-Permian

ABSTRACT

Minute fossils from a variety of different metazoan clades, collectively referred to as small shelly fossils, represent a distinctive taphonomic mode that is most commonly observed in the Cambrian Period. Lower Triassic successions of the western United States, deposited in the aftermath of the end-Permian mass extinction, provide an example of small shelly-style preservation that significantly post-dates Cambrian occurrences. Glauconitized and phosphatized echinoderms and gastropods are preserved in the insoluble residues of carbonates from the Virgin Limestone Member of the Moenkopi Formation. Echinoderm plates, spines and other skeletal elements are replaced; gastropods are preserved as steinkerns. All small shelly-style fossils are preserved in the small size fractions of the residues (177 to 420 μm), which is consistent with the size selection of small shelly fossils in the Cambrian. Energy-dispersive X-ray spectra of individual fossils coupled with X-ray diffraction of residues confirm that the fossils are dominantly preserved by apatite and glauconite. The nucleation of both of these minerals requires that pore water redox oscillated between oxic and anoxic conditions, which, in turn, implies that Lower Triassic carbonates periodically experienced oxygen depletion after deposition and during early diagenesis. Long-term oxygen depletion persisted through the Early Triassic, creating diagenetic conditions that were instrumental in the preservation of small shelly fossils in both Triassic and, likely, Paleozoic examples

INTRODUCTION

Small shelly style preservation is a common mode of preservation in Cambrian deposits worldwide (Brasier, 1990; Dzik, 1994, Porter, 2004). This style of preservation is

characterized by the replacement of skeletal elements, regardless of taxonomic affinity, by apatite and to a lesser extent iron oxides and glauconite (e.g., Brasier, 1990; Porter, 2004; Creveling et al., 2014a, b). These fossils have been well studied from insoluble residues of limestone, and it has been noted that the small size of some of these fossils is a function of the taphonomic process that fostered their preservation (Creveling et al., 2014b). For example, it has been suggested that the size of the organisms likely led to the trapping of phosphorous-rich organic matter in the interstices of the shells, in an environment experiencing periodic oxygen depletion (Creveling et al., 2014b), at least in one Cambrian succession. Small shelly-style preservation is present in the Ordovician (Datillo et al., 2016) and into the Silurian (Dzik, 1994) but their abundance declines after the early Cambrian (Porter, 2004), and they are essentially absent from post-Paleozoic deposits (Dzik, 1994).

The composition of small shelly fossil assemblages changes through the Paleozoic (Dzik, 1994). Early Cambrian assemblages are characterized by a variety of diminutive organisms and remains, some with problematic affinities, which make up the small shelly faunas of this time. Many of these fossils are only known from their phosphatic remnants. In contrast, even by Ordovician time, much of what makes up phosphatized assemblages is also at least broadly reflected in the macrofaunal assemblage, but what appears to constrain phosphatization is the size of the organisms (Datillo et al., 2016). Mollusks are common components of post-Cambrian assemblages, with small adults or juveniles making up much of what is preserved (Dzik, 1994; Datillo et al., 2016).

The decline in abundance of small shelly fossils, and relatedly, phosphatized deposits, after the Cambrian has been linked to the closing of a taphonomic window that operated in the Early Paleozoic (Porter, 2004). This disappearance coincides with

seafloor settings becoming more oxygenated (Sperling et al., 2015), not unlike the distribution of soft-bodied fossils (Allison and Briggs, 1993). However, despite the inference that anoxia played an important role in phosphatization, the geochemical mechanisms behind small shelly-style preservation have remained unclear (e.g., Creveling et al., 2014b).

In the upper Lower Triassic Virgin Limestone Member, Moenkopi Formation of southern Nevada (Figure 1, 2), samples that also preserve silicified fossils (Pruss et al., 2015) contain abundant replaced fossils and internal molds in the small size fractions (250 μm to 420 μm; 177 μm to 250 μm). These fossils are glauconitic and phosphatic echinoderms and gastropods (Figure 3—5); they are identical in mineralogy to small shelly fossil-style preservation of the Cambrian. The gastropods occur as steinkerns of apatite and glauconite. Echinoderm plates and spines are replaced by glauconite and apatite. Rare occurrences of foraminifera, ophiuroid fragments, and ossicles are also glauconitic. These fossils tend to occur in the upper half of the Virgin Limestone Member at both the Ute and Muddy Mountains localities (Figure 2) in shallow water fossiliferous packstone and grainstone samples (Figure 1B). The ubiquity of these fossils in the small size fraction suggests that these Triassic deposits represent a resurgence of Cambrian-style preservation driven by prevailing redox conditions in the sediment during early diagenesis.

GEOLOGIC SETTING

In the Muddy Mountains, the Spathian (upper Lower Triassic) Moenkopi Formation unconformably overlies the carbonates of the Lower Permian Kaibab Formation. The

Moenkopi contains a series of fluvial-marine siliciclastic units with a few dominantly carbonate members (Shorb, 1983). One such example of marine deposition is the Virgin Limestone Member (180 to 190 m-thick), a mixed carbonate-siliciclastic unit, which is well exposed in the Weiser ridge near Overton, and the California ridge near Ute in southern Nevada (Figure 1; Shorb 1983; Pruss et al. 2005). It is constrained to latest early Triassic in age based on ammonoid biostratigraphy (Poborski 1954).

The Virgin Limestone Member has been well studied for both its fossil community composition in the aftermath of mass extinction (Schubert and Bottjer 1995; Fraiser and Bottjer, 2007), the abundance of microbialites (e.g., Schubert and Bottjer, 1992, Pruss and Bottjer, 2004, Mata and Bottjer, 2011), and its silicified faunas (Moffat and Bottjer, 1999). In the more proximal sections of the Virgin Limestone Member in the Muddy Mountains, silicified fossils occur in the upper half of these sections (Pruss et al., 2015). In six of these beds, fossils exhibiting small shelly-style preservation are preserved.

METHODS

A set of 26 samples of fossil packstone and grainstone with silicified fossils were dissolved in 200–400 mL 10% glacial acetic acid solution buffered with ammonium acetate. In six samples, insoluble residues of small size (250 μm to 420 μm; 177 μm to 250 μm) produced replaced echinoderms and internal molds of gastropods. Insoluble residues were examined under a Nikon SMZ645 stereoscopic microscope, and fossils with well-preserved morphology and exhibiting different mineralogical compositions were selected for further analysis. Each fossil was placed on a peg, coated with gold and palladium, and imaged with the scanning electron microscope (SEM). We also used

energy dispersive X-ray spectrometry (SEM-EDS) to determine elemental composition of the samples.

To determine the mineralogical composition of the residues that hosted the fossils, powder X-ray diffraction (XRD) was performed at the University of Oxford on the insoluble residues of all samples that preserved replaced small shelly-style fossils. Powder X-ray diffraction was performed on bulk sample powders by grinding by hand in an agate mortar and pestle. Samples were mounted as a slurry mixed with anhydrous ethanol on a low background scattering silicon crystal substrate and analyzed using a Panalytical Empyrean Series 2 diffractometer operating at 40 kV and 40 mA with a Co Kα source. Samples were analyzed while continuously rotated and data were acquired from 5-85 degrees 2-theta using a step size of 0.026 degrees. Diffraction data were reduced using the HighScore Plus software suite and mineral identifications were based on correspondence to the ICDD Powder Diffraction File 4+ database. In addition, clay mineral speciation and polytype identification were performed by scanning from 69-75 degrees 2-theta using a step size of 0.026 degrees and count rates of 200 seconds per step. In this way, mineral-specific 060 reflections were quantified and clay mineral abundances expressed as a relative fraction of the total clay content, because the area of these reflections has been shown to correspond in a linear fashion to clay mineral abundance (Środoń et al., 2001).

RESULTS

Silicified fossils were found in eleven of the twenty-six residues that were dissolved, but glauconitized and phosphatized fossils were only abundant in six. These fossils are

134 preserved in the small size fractions of the insoluble residues (250 µm to 420 µm; 177
135 µm to 250 µm), and are rare or absent in any size fractions >420 µm. Although
136 glauconite and apatite are visibly present in many of the small sized residues, they occur
137 as grains and do not always replace fossils. Other grains that are glauconitized and
138 phosphatized include ooids and grapestones, but these were not considered in this
139 analysis. Silicified fossils also occur in the small size fractions, but are not as abundant as
140 they were in the larger fractions.

141 The dominant fossils consist of echinoderm spines with replaced stereom by
142 apatite or glauconite (*sensu* Clausen and Smith, 2005) and internal molds of gastropods
143 (Figures 3, 4). Forams, crinoid ossicles, and ophiuroid fragments are rare (Figure 5). The
144 abundance of gastropod steinkerns is a common feature of small shelly-style deposits
145 (e.g., Dzik, 1994; Datillo et al., 2016). Other fossils that were more commonly silicified,
146 such as bivalves (Pruss et al., 2015), are not preserved by glauconite or apatite in these
147 residues or were too fragmented to identify. Most echinoderm material consists of broken
148 skeletal plates and spines likely from crinoids and echinoids. Both planispiral and high-
149 spired gastropods are present, but the granular preservation makes identification beyond
150 class level difficult.

151 Both EDS (energy-dispersive spectra) of individual fossils and XRD of the
152 residues confirm the mineralogic assignments (Figure 6). Green fossils, like the
153 echinoderm spine and foraminiferan, had peaks in EDS spectra corresponding to Si, O,
154 Al, Mg, K and Fe with some Ca and P (Figure 6A, C). The presence of all of these
155 elements is consistent with glauconite; the calcium and phosphorous peaks suggest
156 apatite is also present. Pink or brown fossils, like the gastropod and echinoderm spine,
157 typically had large peaks at Ca and P (Figure 6B, D), suggesting a composition of apatite.

X-ray diffraction analysis of the residues that hosted the fossils reveal the presence of glauconite and apatite, and that they are each absent in only one residue (VMM12-42 and VMM16-46A, respectively; Figure 7, Table 1). Other minerals of varying abundance include quartz and plagioclase with trace amounts of goethite, pyrite, and kaolinite (Table 1).

DISCUSSION

Echinoderm fragments and gastropods are the most common small shelly fossils of the Virgin Limestone Member, and these occur in the 250 μm to 420 μm and 177 μm to 250 μm size fractions. Interestingly, and unlike the Cambrian small shellies, small shelly-style fossils in Lower Triassic rocks are remnants of taxa that are also preserved as large fossils. This suggests that this taphonomic window does not necessarily capture an unknown diversity as it does in the Cambrian but rather simply reflects the reemergence of a style of preservation that is generally rare after the Paleozoic (Dzik, 2004). The fragments preserved by glauconite and apatite are members of the same groups (crinoids, echinoids, ophiuroids, and gastropods) that are described from Early Triassic ecosystems globally. It is possible that a supply of small organisms in the Early Triassic is related to the Lilliput Effect, that has been widely described from this interval of time (e.g., Twitchett, 2007), but it seems more likely that this style of preservation can occur at any time that environmental conditions are conducive to it (Creveling et al. 2014b).

The Role of Redox Oscillations in Fossil Preservation

Small shelly style preservation has been extensively documented from rocks of the Cambrian (Brasier, 1990; Dzik, 1994, Porter, 2004), and to a lesser degree in Ordovician deposits (Datillo et al., 2016) and the remainder of the Paleozoic (Dzik, 1994). In particular, widespread phosphatic deposits characterize the Ediacaran and Cambrian periods, including the Doushanto Formation; some of these exceptionally preserve fossils (e.g., Zhang et al., 1998). Small shelly fossils are essentially unknown from the post-Paleozoic fossil record, and previous authors have attributed this pattern to the closing of a taphonomic window that allowed for the preservation of fossils in this way (Porter, 2004). In the Lower Triassic Virgin Limestone Member, the abundance of phosphatized and glauconitized fossils suggest a local return to Cambrian style preservation in these units. But what factors might have contributed to the re-opening of this taphonomic window in the Lower Triassic?

The presence of small shelly-style fossils in Lower Triassic carbonates suggests an intermittent return to Cambrian-style diagenesis (e.g., Pruss et al., 2004, 2005). Recent work on the taphonomy of Cambrian small shelly fossils from Australia showed that steinkerns commonly form through phosphatization (Creveling et al., 2014b) by remobilization of phosphorous under locally anoxic conditions (Creveling et al., 2014a). In addition to the phosphatic fossils found in the Virgin Limestone, there is also an abundance of glauconitized fossils. The occurrence of both glauconite and apatite provides important constraints on the nature of pore water geochemistry, mineralization, and SSF preservation in the Virgin Limestone.

The abundant occurrence of glauconite, a redox-sensitive Fe-rich authigenic clay mineral, reflects the initial precipitation of Fe-rich smectite from pore water, and redox conditions that oscillated between oxic and anoxic. These prerequisites for glauconite

206 formation arise because as Fe in authigenic Fe(II)-smectite is oxidized and then re-
207 reduced in response to redox fluctuations, irreversible structural alterations act to increase
208 K content, increase Fe(II) content, which together act to decrease interlayer expandability
209 (Khaled and Stucki, 1991; Shen and Stucki, 1994; Gorski et al., 2013; Neumann et al.,
210 2011). Thus, with each oscillation in pore water redox, authigenic Fe-smectite precursors
211 become progressively converted to glauconite (Khaled and Stucki, 1991; Shen and Stucki,
212 1994), the rate of which is a direct function of the rate of redox oscillation. From this
213 perspective, it is easier to understand why, as discussed above, fluctuations in redox state
214 of the interiors of organic-rich particles of a given size range are more likely to produce
215 glauconite, at least in the presence of sufficient Fe, Mg and $SiO_2(aq)$ to promote the
216 initial precipitation of Fe-smectite precursors. Indeed, glauconite is well known as an
217 abundant and ubiquitous component of fecal pellets and irregular organic-rich grains and
218 aggregates, highlighting a well-known mineralogical expression of the dynamic redox
219 evolution of a wide variety of organic-rich microsystems (Boyer et al., 1977; Odin and
220 Matter, 1981).

221 The abundance of glauconite in particle interiors in turn provides crucial insight
222 into the cycling of PO_4 in Virgin Formation sediments, and therefore the precipitation of
223 apatite. The PO_4 localized in apatite was likely provided by P liberated from organic
224 matter and/or from the shuttling of Fe, whereby adsorbed P on Fe-oxide particles is
225 released and locally concentrated where redox cycling occurs (Berner, 1973; Krom and
226 Berner, 1981; Slomp et al., 1996). Indeed, a sedimentary Fe source and oscillating redox
227 reflected by glauconite would have amplified the efficiency of PO_4 delivery and
228 concentration in small shelly microenvironments through redox cycling. In addition to
229 Fe-associated PO_4, previous work has shown that oscillating redox tends to promote P

storage in organic matter, relative to fully anoxic sediments (Aller, 1994). Together, redox oscillations would have promoted increased PO_4 concentrations in particle interiors from both Fe-associated and organic-associated sources.

Although redox oscillations were clearly important in concentrating PO_4 at the local scale in Virgin Limestone SSFs, the precipitation of carbonate-fluoro-apatite (CFA) requires the availability of CO_3^{2-}, which is closely coupled to pH. On the basis of this requirement, Creveling et al. (2014b) suggested that, in the presence of sufficient sedimentary PO_4 sources, relatively low SO_4 concentrations would have helped promote CFA nucleation because of the acidifying effects of microbial sulfate reduction. Thus, greater proportions of reducible Fe relative to SO_4 would promote enhanced Fe reduction, in turn increasing pore water pH, making CO_3^{2-} more available, and increasing CFA supersaturation. The abundance of glauconite perhaps reflects a greater role for Fe reduction in buffering pore water pH relative to SO_4 reduction, in particular if marine SO_4 concentrations were lower in the Triassic than modern seawater (Song et al., 2014). Although modern diagenetic studies indicate that redox oscillations may have promoted complex dynamic changes in the availability of oxidants and in pore water pH (Zhu et al., 2006), low pore water SO_4 may have been a key prerequisite that helped promote the formation of apatite in addition to glauconite in Virgin Limestone SSFs.

In summary, glauconite and apatite associated with SSFs indicate that redox oscillations within shell interiors played a key role in generating both minerals. Redox fluctuations drove glauconitization of precursor Fe-smectite, which itself reflects an important source of Fe to Virgin Limestone sediments. These fluctuations enhanced PO_4 accumulation in shell interiors through redox cycling of particulate Fe minerals and/or the preferential accumulation, and eventual release, of P associated with organic matter.

Size selection of Early Triassic small shelly-style fossils

The echinoderms have stereom replaced by apatite and glauconite, often in the same samples where the larger fractions hosted silicified examples (Pruss et al., 2015). It is possible that the abundance of organic matter in the stereom, which has been known to play a role in silicification of fossils, fostered glauconitization and phosphatization of echinoderms in these assemblages, (e.g., Butts 2014; Butts and Briggs 2010, Pruss et al., 2015). However, there must be other factors at play because glauconitized and phosphatized fossils are nearly absent from the larger size fractions (>420 μm). The gastropods follow a similar pattern of preservation to Early Paleozoic small shelly assemblages with an abundance of steinkerns in these Triassic residues (Creveling et al., 2014b; Datillo et al., 2016). The steinkerns are thought to reflect external sources of phosphate (Wilby and Briggs 1997), with some nucleation on existing organic material (Creveling et al., 2014a, b). The preservation of these fossils in the smallest size fractions suggests that selectivity relating to size is operating (Creveling et al., 2014b) even relative to silicified fossils in the same assemblages (silicified fossils are typically 1 mm or larger).

One way to understand why SSF preservation in the Virgin Limestone is associated with a size selection is to consider the controls on the redox state of the interior of the shells or fossils themselves. Jahnke (1985), following Jorgensen (1977) constructed a simple model to interpret pore water profiles of oxygen and nitrogen species in deep-sea sediments by treating particles containing organic matter as simple spheres. In this model, the redox state of the interior (or, more precisely, the conditions

for anoxia to develop at the center of the particle) is a function of the effective radius of the particle (R), the diffusion coefficient within the particle (D, or the value incorporating chemical diffusivity across organic membranes, etc.), the $O_2(aq)$ content of the surrounding pore water (C), and the rate of $O_2(aq)$ consumption within the particle (J), which is determined by the net rate of $O_2(aq)$-consuming metabolic reactions for a given microbial ecology. Anoxia will develop in the center of the particle when the radius of the particle, R,:

$$R=(6DC/J)^{0.5}$$

Figure 8 plots this relationship at two different pore water $O_2(aq)$ concentrations. It is clear from this relationship that, for any given rate of $O_2(aq)$ consumption and $O_2(aq)$ content of the surrounding pore water, there will be a size limit above which the interior of the particle will be continuously anoxic. Similarly, particles that are below a given $O_2(aq)$ consumption rate, or below the resolution of our analytical techniques, will be continuously oxic or be characterized by a redox state identical to that of the surrounding pore water. This is simply because particles below a given size limit do not contain enough organic matter to overcome the diffusion of $O_2(aq)$ from surrounding pore water to the particle center. However, particles within these two end member sizes will be characterized by redox conditions that are poised close to the anoxic/oxic boundary. It follows that oscillations in the redox state of the interiors of particles within this size range will be likely to occur in response to small variations in any combination of local $O_2(aq)$ content, metabolic $O_2(aq)$ consumption rate, or changes in the diffusivity of the interior. Importantly, Figure 8 also shows that as the $O_2(aq)$ concentration of the pore water decreases, so too does the particle size window at which redox oscillations are likely to occur. Thus, lower pore water O_2(aq) selects for smaller particle sizes that are

more likely to experience redox oscillations during deposition and early diagenesis.

These simple calculations examining the development of particle anoxia indicate that low $O_2(aq)$ in sediment pore water exerted a size selection on particles likely to experience redox oscillations at a given metabolic ($O_2(aq)$ consumption) rate. In addition, low marine, and therefore, low pore water SO_4 concentrations, combined with sufficient reducible sedimentary Fe, allowed pH to increase upon microbial mineralization of organic matter. This, in turn, allowed CO_3^{2-} concentrations to rise, driving increased supersaturation of CFA in the particles themselves. Together, these conclusions imply that SSF preservation during Virgin Limestone sedimentation and diagenesis was, above all else, a strong function of low pore water $O_2(aq)$ and low SO_4.

It is possible, in light of the fossils preserved here, that there are other intervals of the Phanerozoic that might contain fossils preserved in a similar way. For example, in addition to the abundance of glauconitic and phosphatic deposits of the Cambrian, the Cretaceous contains abundant glauconite worldwide (Peters and Gaines, 2012). Local examples show widespread glauconite associated with phosphorites during warm, low oxygen conditions (Glenn and Arthur, 1988). Since warm epicontinental seas were occasionally present throughout the Cretaceous, this may be yet another interval that contains small shelly-style preservation of fossils, given that conditions were right for glauconitic and phosphatic deposits.

Environmental conditions of the Early Triassic

The end-Permian mass extinction triggered a delayed recovery for 5 million years following the event (e.g., Erwin, 2001), and this interval of time is characterized by long-

326 term environmental stress. For example, the Early Triassic experienced large-scale
327 oscillations in the carbon isotope record potentially linked to periodic volcanism (Payne
328 and Kump, 2007), lethally hot ocean temperatures (Sun et al., 2012), and evidence for
329 sustained anoxia (e.g., Isozaki, 1997; Grice et al., 2005; Grasby et al., 2013). Lower
330 Triassic glauconitic and phosphatic deposits are known from high latitude successions,
331 like the Vardebukta Formation (Wignall et al., 1998) and Vikinghøgda formations
332 (Mørk et al., 1999) of Svalbard, and lesser amounts in low latitude outer shelf settings,
333 like Aggtelek Karst, Hungary (Hips, 1999), but they are quantitatively rare when
334 normalized to rock volume and compared to other time intervals (Peters and Gaines,
335 2012). Nonetheless, their presence in Lower Triassic successions points to conditions, at
336 least in some areas, which were conducive to the formation glauconitic and phosphatic
337 deposits.

338 It is generally accepted that offshore environments of the Early Triassic
339 experienced low oxygen conditions, perhaps for millions of years (e.g., Isozaki, 1997;
340 Grice et al., 2005; Grasby et al., 2013; Song et al., 2014). What has been less well known
341 is the degree to which low oxygen waters affected shelf environments, and reports have
342 put forth equivocal views (e.g., Twitchett et al., 2004; Lau et al., 2016). Here, the
343 presence of glauconitized and phosphatized fossils in these facies suggests that the
344 sediments of the Lower Triassic Virgin Limestone experienced oscillating redox during
345 early diagenesis after burial, which, in turn, fostered small shelly-style preservation. In
346 addition to oscillating background oxygen levels, Lower Triassic sediments have been
347 widely viewed as poorly ventilated because of conspicuously low levels of bioturbation
348 (Buatois and Mángano, 2011), related to small trace fossils coupled with low ichnofabric

indices (Pruss and Bottjer, 2004). Other indicators of suppressed animal activity include the preservation of wrinkle structures and other microbialites worldwide (Pruss et al., 2004). We prefer the notion that poorly ventilated sediments allowed for redox oscillations rather than local organic loading, since shallow water sections of the Lower Triassic, including the units examined here, are notoriously lean with respect to organic carbon (Krull et al., 2004; Marenco et al., 2012). Small shelly-style fossilization in these Triassic sediments indicates that environmental conditions that also brought about a long-term delayed recovery from the end-Permian mass extinction promoted diagenetic reactions that controlled the styles of fossilization.

CONCLUSIONS

Small shelly fossils of the Lower Triassic Virgin Limestone offer valuable insight into the specific diagenetic conditions that controlled the spatial and temporal distribution of this taphonomic mode. The mineralogical composition of these fossils unambiguously reflects periodically low oxygen content of sediment pore waters. Because these conditions persisted for 5 million years beyond the end-Permian mass extinction, Lower Triassic carbonates offer a new opportunity to examine the diagenetic consequences of Earth's largest mass extinction and its delayed recovery. Finally, the resurgence of small shelly-style fossils in the Lower Triassic helps explain the closing of this taphonomic window in the Cambrian. Global geochemical datasets reflect a shift to oxygenated conditions well into the later Paleozoic (Sperling et al., 2015), so as seafloors became progressively ventilated, redox oscillation became less common and so too did the early diagenetic precipitation of glauconite and/or phosphate – mineral substrates that each

373 reflect a dynamic sedimentary redox landscape.

374

375 **ACKNOWLEDGEMENTS**

376 SP and CS acknowledge helpful conversations with P. Wignall and S. Westacott, a
377 helpful review from B. Datillo on an earlier version of this manuscript, and field
378 assistance from T. Browne, J. Chang, C. Deeg, K. Klema, J. Loveless, C. Mwinde, E.
379 Roth, E. Smith, H. Tatgenhorst, and Z. Zhang. We thank the Smith College Department
380 of Geosciences for funding for field work.

381

REFERENCES CITED

ALLER, R.C., 1994, Bioturbation and remineralization of sedimentary organic matter: effects of redox oscillation: Chemical Geology, v. 114, p. 331—45

ALLISON, P.A., AND BRIGGS, D.E.G., 1993, Exceptional fossil record: Distribution of soft-tissue preservation through the Phanerozoic: Geology, v. 21, p.527–530.

BERNER, R.A., 1973, Phosphate removal from sea water by adsorption on volcanogenic ferric oxides: Earth and Planetary Science Letters, v. 18, p. 77–86.

BOYER, P.S., GUINNESS, E.A., LYNCH-BLOSSE, M.A. AND STOLZMAN, R.A., 1977, Greensand fecal pellets from New Jersey: Journal of Sedimentary Research, v. 47, p. 267–280.

BRASIER, M. L., 1990, Phosphogenic events and skeletal preservation across the Precambrian-Cambrian boundary interval: Geological Society of London, Special Publications, v. 52, p. 289—303.

BUATOIS, L. A., AND MÁNGANO, M. G., 2011, The déjà vu effect: Recurrent patterns in exploitation of ecospace, establishment of the mixed layer, and distribution of matgrounds: Geology, v. 39, p. 1163—1166.

BUTTS, S.H., 2014, Silicification: LaFlamme, M., Schiffbauer, J.D., and Darroch, S.A.F.: Reading and writing of the fossil record: Preservational Pathways to Exceptional Fossilization: Paleontological Society Short Course, v. 20, p. 15–33.

BUTTS, S.H., AND BRIGGS, D.E., 2010, Silicification through time, *in* Allison, P. and Bottjer, D.J. eds., Taphonomy: Process and Bias Through Time, Springer, Berlin, p. 411–434.

CLAUSEN, S., AND SMITH, A. B., 2005, Palaeoanatomy and biological affinities of a Cambrian deuterostome (Stylophora): Nature, v. 438, p. 351–354.

406 CREVELING, J.C., JOHNSTON, D.T. POULTON, S.W, KOTRC, B., MARZ, C., SCHRAG, D.P.,
407 AND KNOLL, A.H., 2014a, Phosphorus sources for phosphatic Cambrian
408 carbonates: Geological Society of America Bulletin, v. 126, p. 145–163.
409 CREVELING, J.C., KNOLL, A. H., AND JOHNSTON, D. J., 2014b, Taphonomy of Cambrian
410 small shelly fossils: PALAIOS, v. 29, p. 295–308.
411 DATILLO, B., FREEMAN, R.L., PETERS, W.S., HEIMBROCK, W.P., DELINE, B., MARTIN, A.J.,
412 KALLMEYER, J.W., REEDER, J., ARGAST, A., 2016, Giants among micromorphs:
413 were Cincinnatian (Ordovician, Katian) small shelly phosphatic faunas dwarfed?:
414 PALAIOS, v. 31, p. 55–70.
415 DZIK, J., 1994, Evolution of 'small shelly assemblages' of the Early Paleozoic: Acta
416 Palaeontologica Polonica, v. 39, p. 247–313.
417 ERWIN, D.H., 2001, Lessons from the past: Biotic recoveries from mass extinctions:
418 Proceedings of the National Academy of Sciences, v. 98, p. 5399–5403.
419 FRAISER, M. L., AND BOTTJER, D. J., 2007, When bivalves took over the world:
420 Paleobiology, v. 33, p.397–413.
421 GLENN, C.R., AND ARTHUR, M.A., 1988, Petrology and major element geochemistry of
422 Peru margin phosphorites and associated diagenetic minerals: authigenesis in
423 modern organic-rich sediments: Marine Geology, v. 80, p. 231–67.
424 GORSKI, C.A., KLÜPFEL, L.E., VOEGELIN, A., SANDER, M. & HOFSTETTER, T.B., 2013,
425 Redox Properties of Structural Fe in Clay Minerals: 3. Relationships between
426 Smectite Redox and Structural Properties: Environmental Science and
427 Technology, v. 47, p. 13477–85.
428 GRASBY, S. E., BEAUCHAMP, B., EMBRY, A., AND SANEI, H., 2013, Recurrent Early
429 Triassic anoxia: Geology, v. 41, no. 2, p. 175-178.

GRICE, K., CAO, C., LOVE, G.D., BÖTTCHER, M.E., TWITCHETT, R.J., GROSJEAN, E., SUMMONS, R.E., TURGEON, S.C., DUNNING, W., AND JIN, Y., 2005, Photic zone euxinia during the Permian-Triassic superanoxic event: Science, v. 307, is. 5710, p. 706–709.

HIPS, K., 1999, Lower Triassic storm-dominated ramp sequence in northern Hungary: an example of evolution from homoclinal through distally steepened ramp to Middle Triassic flat-topped platform: Geological Society of London Special Publications, v. 159, p. 315–338.

ISOZAKI, Y., 1997, Permo–Triassic boundary superanoxia and stratified superocean; records from lost deep sea: Science, v. 276. p. 235–238.

JAHNKE, R., 1985, A model of microenvironments in deep-sea sediments: formation and effects on porewater profiles: Limnology and Oceanography, v. 30, p. 956–65

JØRGENSEN, B. B., 1977, Bacterial sulfate reduction within reduced microniches of oxidized marine sediments: Marine Biology, v. 41, p. 7–17.

KHALED, E.M. & STUCKI, W., 1991, Iron Oxidation State Effects on Cation Fixation in Smectites: Soil Scientific Society of America Journal, v. 551550, p. 550

KROM, M.D. & BERNER, R.A., 1981, The diagenesis of phosphorus in a nearshore marine sediment, *Geochimica et Cosmochimica Acta*, 45(2), pp. 207–16

KRULL, E. S., D. J. LEHRMANN, D. DRUKE, B. KESSEL, Y. YU, AND R. LI, 2004, Stable carbon isotope stratigraphy across the Permian–Triassic boundary in shallow-marine carbonate platforms, Nanpanjiang Basin, south China: Palaeogeography, Palaeoclimatology, Palaeoecology, v. 204, no. 3–4, p. 297–315.

452 LAU, K.V., MAHER, K., ALTINER, D., KELLEY, B.M., KUMP, L.R., LEHRMANN, D.J.,
453 SILVA-TAMAYO, J.C., WEAVER, K.L., YU, M., AND PAYNE, J.L., 2016, Marine
454 anoxia and delayed Earth system recovery after the end-Permian extinction:
455 Proceedings of the National Academy of Sciences, v. 113, p. 2360–65.
456 MARENCO, P. J., GRIFFIN, J. M., FRAISER, M. L., AND CLAPHAM, M. E., 2012,
457 Paleoecology and geochemistry of Early Triassic (Spathian) microbial mounds
458 and implications for anoxia following the end-Permian mass extinction: Geology,
459 v. 40, p. 715–8.
460 MATA, S. A., AND BOTTJER, D. J., 2009, The paleoenvironmental distribution of
461 Phanerozoic wrinkle structures: Earth-Science Reviews, v. 96, p. 181–195.
462 MØRK, A., ELVEBAKK, G., FORSBERG, A. W., HOUNSLOW, M. W., NAKREM, H. A.,
463 VIGRAN, J. O. AND WEITSCHAT, W. 1999. The type section of the Vikinghøgda
464 Formation: a new Lower Triassic unit in central and eastern Spitsbergen: Polar
465 Research v., 18, p. 51–82.
466 MOFFAT, H. A., AND BOTTJER, D. J., 1999, Echinoid concentration beds: two examples
467 from the stratigraphic spectrum: Palaeogeography, Palaeoclimatology,
468 Palaeoecology, v. 149, p. 329–348.
469 NEUMANN, A., SANDER, M. & HOFSTETTER, T.B. 2011, Redox Properties of Structural Fe
470 in Smectite Clay Minerals: Aquatic Redox Chemistry, American Chemical
471 Society, p. 361–379.
472 ODIN, G.S., AND MATTER, A., 1981, De glauconiarum origine: Sedimentology, v. 28, p.
473 611–641.

474 PAYNE, J.L., AND KUMP, L.R., 2007, Evidence for recurrent Early Triassic massive
475 volcanism from quantitative interpretation of carbon isotope fluctuations: Earth
476 and Planetary Science Letters, v. 256, p. 264–277.
477 PETERS, S. E., AND GAINES, R. 2012, Formation of the 'great unconformity' as a trigger
478 for the Cambrian explosion: Nature, v. 484, p. 363–366. doi:10.1038/nature10969.
479 POBORSKI, S.J., 1954, Virgin Formation (Triassic) of the St. George, Utah, area:
480 Geological Society of America Bulletin. v. 65, p. 971–1006.
481 PORTER, S.M., 2004, Closing the phosphatization window: testing for the influence of
482 taphonomic megabias on the pattern of small shelly fossil decline: PALAIOS, v.
483 19, p. 178–183.
484 PRUSS, S.B., AND BOTTJER, D.J., 2004, Early Triassic trace fossils of the western United
485 States and their implications for prolonged environmental stress from the end-
486 Permian mass extinction: PALAIOS, v. 19, p. 559–571.
487 PRUSS, S.B., CORSETTI, F.A., AND BOTTJER, D.J., 2005, The unusual sedimentary rock
488 record of the Early Triassic: A case study from the southwestern United States:
489 Palaeogeography, Palaeoclimatology, Palaeoecology, v. 222, p. 33– 52.
490 PRUSS, S.B., FRAISER, M.L., BOTTJER, D.J., 2004, Proliferation of Early Triassic wrinkle
491 structures: Implications for environmental stress following the end-Permian mass
492 extinction: Geology. v. 35, no. 5, p. 461–465.
493 PRUSS, S.B., PAYNE, J.L., WESTACOTT, S., 2015, Taphonomic bias of selective
494 silicification revealed by paired petrographic and insoluble residue analysis:
495 PALAIOS, v. 30, p. 620–626.
496 SCHUBERT, J. K., AND BOTTJER, D. J., 1992, Early Triassic stromatolites as
497 post-mass extinction disaster forms: Geology, v. 20, 883–886.

498 SCHUBERT, J. K., AND BOTTJER, D. J., 1995, Aftermath of the Permian–Triassic mass
499 extinction event: Paleoecology of Lower Triassic carbonates in the Western USA:
500 Palaeogeography, Palaeoclimatology, Palaeoecology, v. 116, p. 1–39.
501 SHEN, S. AND STUCKI, J., 1994, Effects of iron oxidation state on the fate and behavior of
502 potassium in soils: Soil testing: Prospects for improving nutrient
503 recommendations, p. 173–85
504 SHORB, W.M., 1983, Stratigraphy, facies analysis and depositional environments
505 of the Moenkopi Formation (Lower Triassic), Washington County, Utah, and
506 Clark and Lincoln counties, Nevada [MS. thesis]: Durham, North Carolina,
507 Duke University, 205 p.
508 SLOMP, C.P., VAN DER GAAST, S.J. & VAN RAAPHORST, W., 1996, Phosphorus binding by
509 poorly crystalline iron oxides in North Sea sediments: Marine Chemistry, v. 52, p.
510 55–73.
511 SONG, H., TONG, J., ALGEO, T. J., SONG, H., QIU, H., ZHU, Y., TIAN, L., BATES, S., LYONS,
512 T. W., LUO, G., AND JKUMP, L. R., 2014, Early Triassic seawater sulfate
513 drawdown: Geochimica et Cosmochimica Acta, v. 128. p. 95–113.
514 SPERLING, E.A., WOLOCK, C.J., MORGAN, A.S., GILL, B.C., KUNZMANN, M., HALVERSON,
515 G.P., MACDONALD, F.A., KNOLL, A.H., AND JOHNSTON, D.T., 2015, Statistical
516 analysis of iron geochemical data suggests limited Late Proterozoic
517 oxygenation: Nature, v. 523, p. 451–454.
518 ŚRODOŃ J., DRITS V.A., MCCARTY D.K., HSIEH J.C., AND EBERL D.D., 2001, Quantitative
519 x-ray diffraction analysis of clay-bearing rocks from random preparations: Clays
520 and Clay Minerals, v. 49, p. 514–528.

SUN, Y., JOACHIMSKI, M.M., WIGNALL, P.B., YAN, H., CHEN, Y., JIANG, H., XANG, L., AND LAI, X., 2012, Lethally hot temperatures during the Early Triassic: Science, v. 338, p. 366–370.

TWITCHETT, R.J., KRYSTYN, L., BAUD, A., WHEELEY, J.R., AND RICHOZ, S., 2004, Rapid marine recovery after the end-Permian mass-extinction event in the absence of marine anoxia: Geology, v. 32, p. 805–808.

TWITCHETT, R. J., 2007, The Lilliput effect in the aftermath of the end-Permian extinction event: Palaeogeography, Palaeoclimatology, Palaeoecology, v. 252, p. 132–144.

WIGNALL, P. B., MORANTE, R. AND NEWTON, R. 1998. The Permo-Triassic transition in Spitsbergen: δ13Corg. chemostratigraphy, Fe and S geochemistry, facies, fauna and trace fossils: Geological Magazine, v. 133, p. 47–62.

WILBY, P.R., AND BRIGGS, D.E.G., 1997, Taxonomic trends in the resolution of detail preserved in fossil phosphatized soft tissues: Geobios, v. 30, no. 1, p. 493–502.

ZHANG, Y., LEIMING Y., XIAO, S., AND A.H. KNOLL, 1998, Permineralized fossils from the terminal Proterozoic Doushantuo Formation, South China: Journal of Paleontology, v. 72, no. 4, p. 1–52.

ZHU, Q., ALLER, R.C. & FAN, Y., 2006, Two-dimensional pH distributions and dynamics in bioturbated marine sediments: Geochimica et Cosmochimica Acta, 70, p. 4933–49.

FIGURE CAPTIONS

Figure 1: Locality map and stratigraphic columns. A) Map showing location of the outcrops of the Virgin Limestone Member (36°36’01 N, 114°32’57 W, Muddy Mountains Overton locality; 36°32’51 N, 114°36’50 W, Muddy Mountains Ute locality). B) Stratigraphic columns showing all dissolved samples with location of small-shelly fossil samples in bold.

Figure 2: Field photographs of Virgin Limestone Member exposed at A) Muddy Mountains Ute locality; and B) Overton locality. Photographs show upper Virgin Limestone at both localities, containing fossil-bearing beds. Note that both sections are overturned.

Figure 3: Scanning electron microscope (SEM) images of replaced and possible stereomic molds of echinoderm spines from the Virgin Limestone Formation.

Figure 4: Scanning electron microscope images of internal molds of gastropods from the Virgin Limestone Formation.

Figure 5: Scanning electron images of less common fossils found in residue. A) crinoid ossicle; B) foraminifera; and C) ophiuroid fragment.

Figure 6: Energy dispersive spectra (EDS) of representative fossils. A) Echinoderm spine shows peaks in Si, Al, Mg, K, and Fe, with minor Ca and P, all consistent with the minerals glauconite and apatite, respectively. B) Internal mold of a gastropod with abundant Ca and P, consistent with apatite. C) Foraminifera, showing spectra consistent with glauconite and apatite. D) Echinoderm spine showing abundance of Ca and P, with minor K and Fe, suggesting presence of apatite and minor Fe-bearing minerals.

Figure 7: Identification of minerals in Virgin Limestone residues by X-ray diffraction (XRD). A) XRD profile from sample VU12-33 showing high abundances of glauconite

565 (indicated) and apatite (dashed lines). Quartz and calcite peaks are also indicated. B)
566 Zoomed in XRD profile from sample VU12-33 showing how glauconite, illite, and
567 berthierine are identified. Quartz peak is also indicated.
568 Figure 8: Diagram showing particle radius versus oxygen consumption rate using the
569 model of Jahnke (1985), following Jorgensen (1977). Note that the size of small shelly-
570 style fossils in the Virgin Limestone assemblage fall along the region of redox
571 fluctuations in an ambient low oxygen pore water environment.
572 Table 1: X-ray diffraction (XRD) data for the 6 residues that produced abundant
573 phosphatized and glauconitized fossils. Apatite and/or glauconite are present in all
574 residues.
575

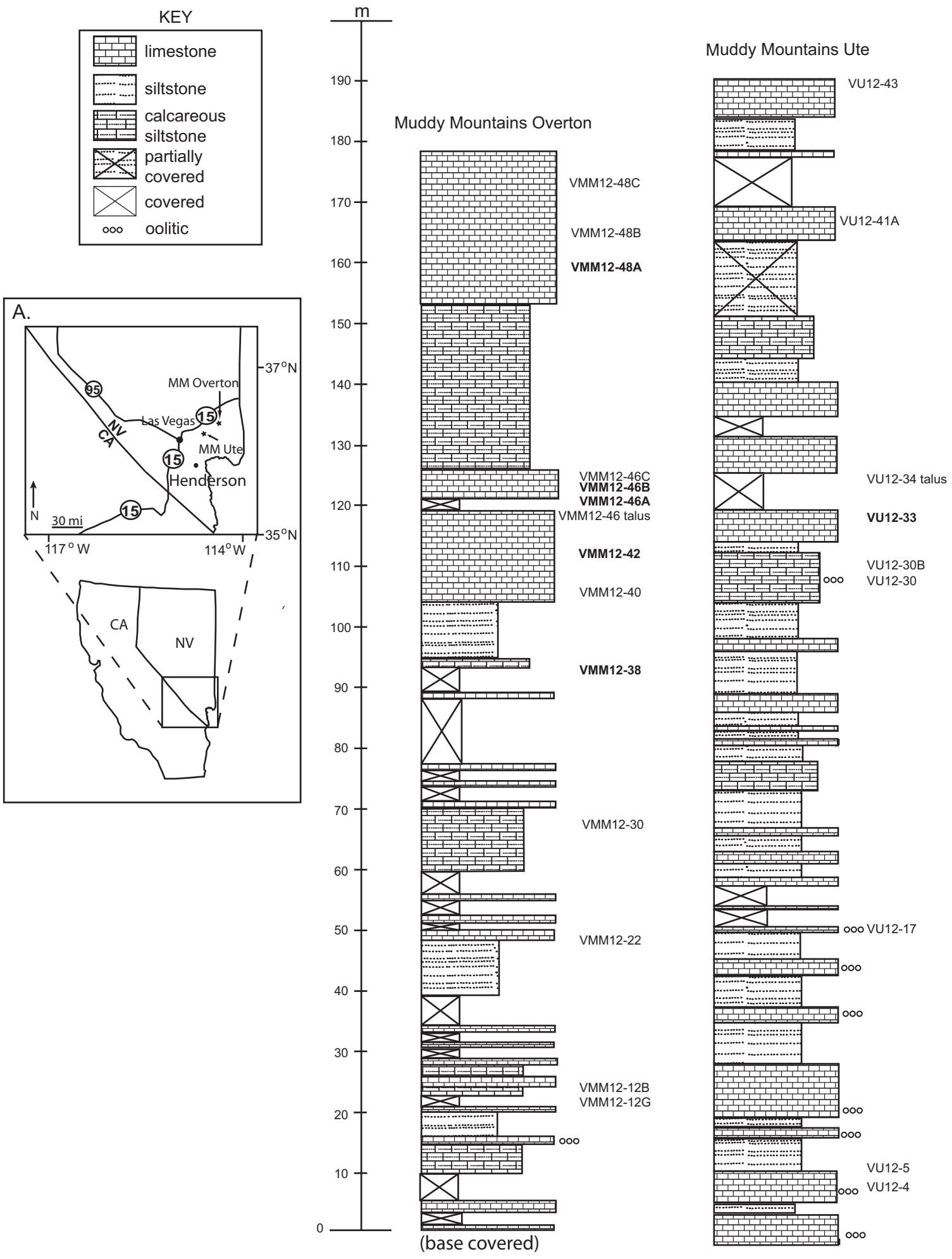
KEY
limestone
siltstone
calcareous siltstone
partially covered
covered
oolitic
A.
37°N
35°N
117° W
114° W
MM Overton
Las Vegas
MM Ute
Henderson
95
15
NV
CA
N
30 mi
B.
Virgin Limestone Member
m
Muddy Mountains Overton
Muddy Mountains Ute
VMM12-48C
VMM12-48B
VMM12-48A
VMM12-46C
VMM12-46B
VMM12-46A
VMM12-46 talus
VMM12-42
VMM12-40
VMM12-38
VMM12-30
VMM12-22
VMM12-12B
VMM12-12G
(base covered)
VU12-43
VU12-41A
VU12-34 talus
VU12-33
VU12-30B
VU12-30
VU12-17
VU12-5
VU12-4

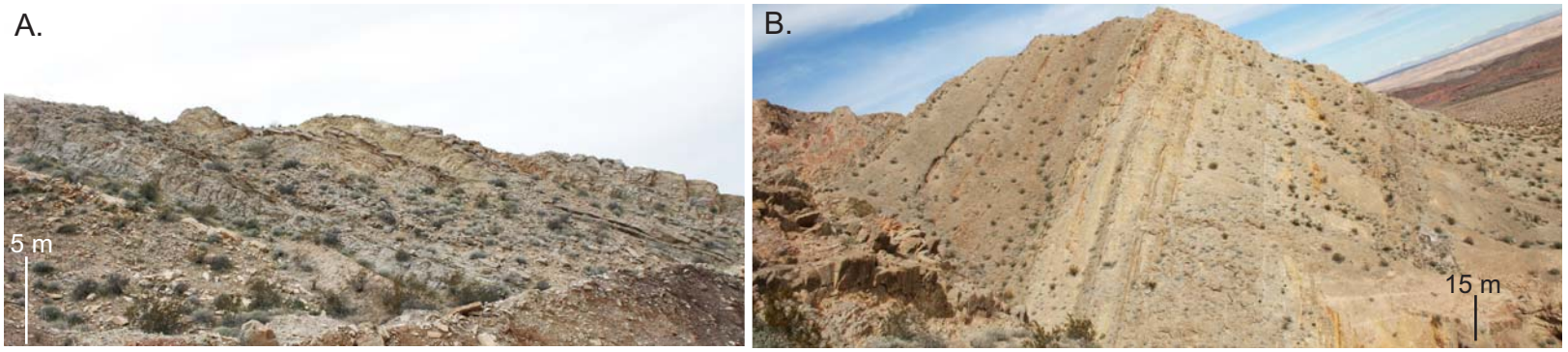
A.
5 m
B.
15 m

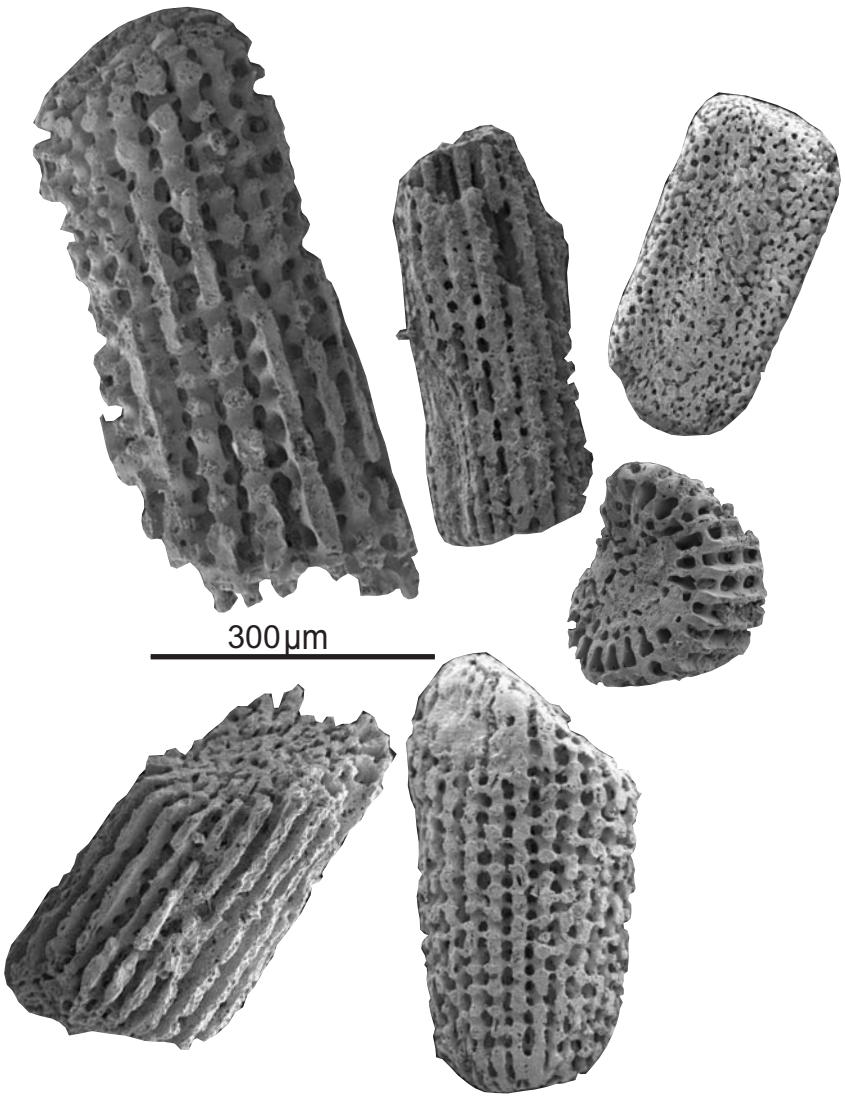
300 µm

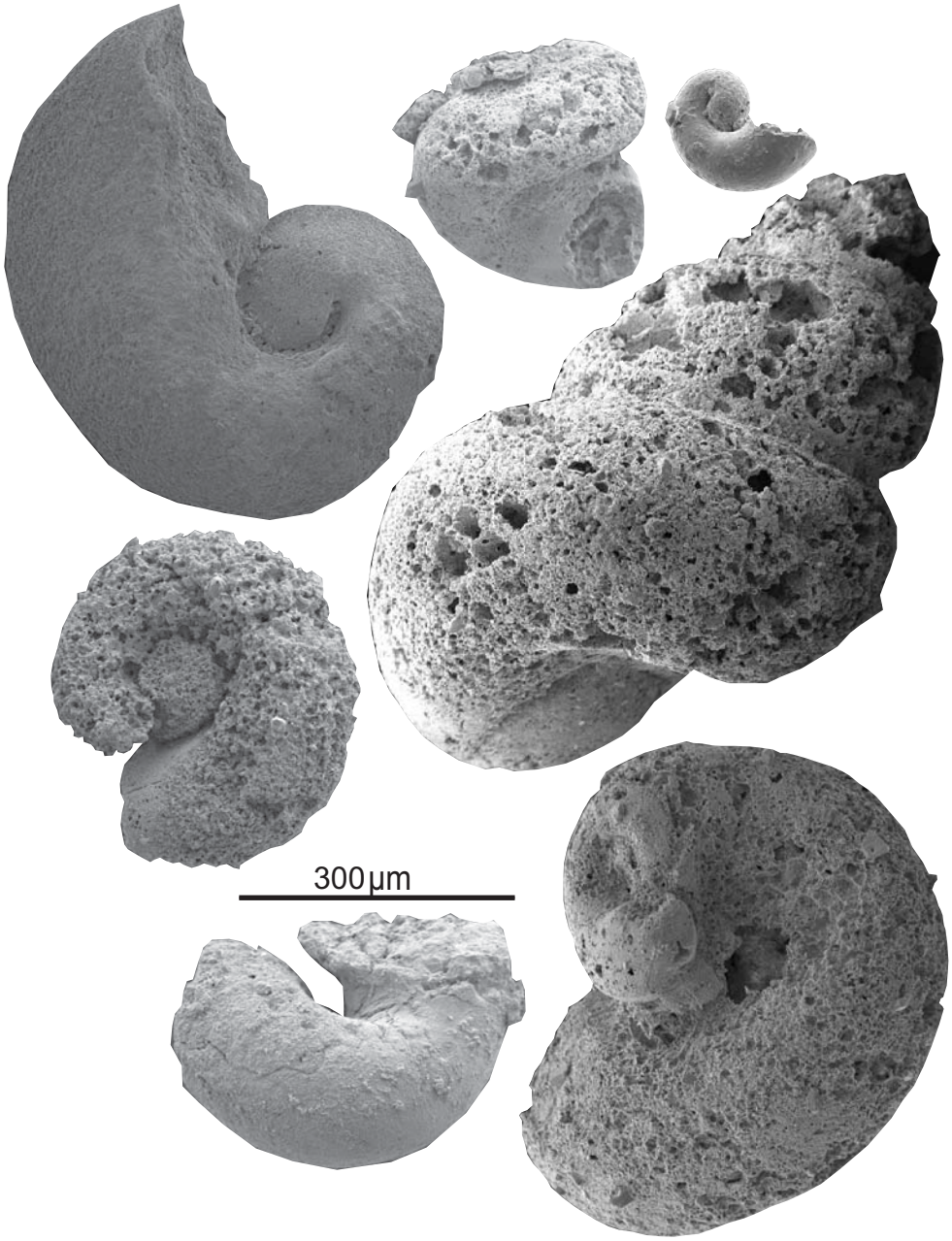
300 µm

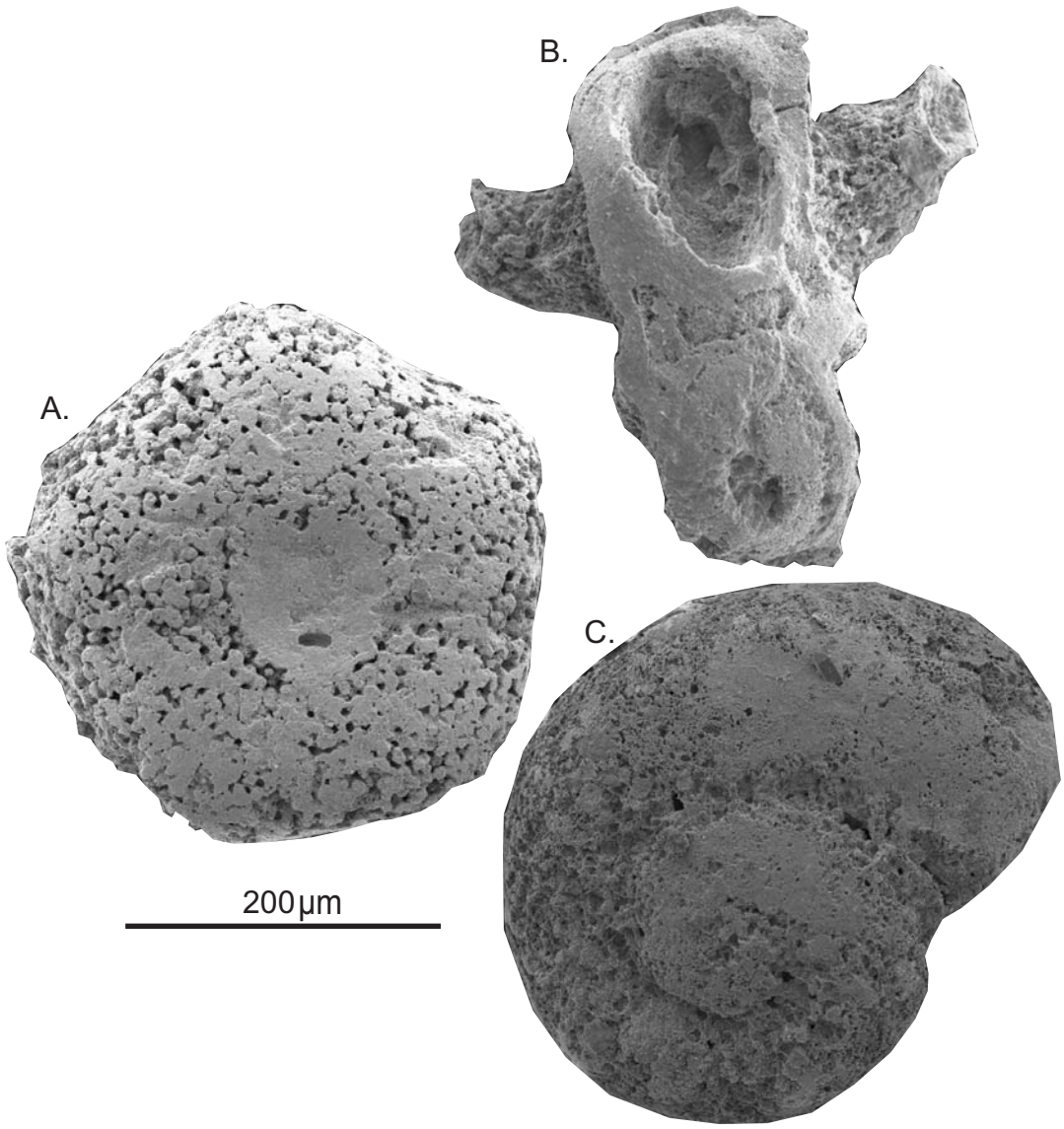
B.
A.
C.
200 µm

A.

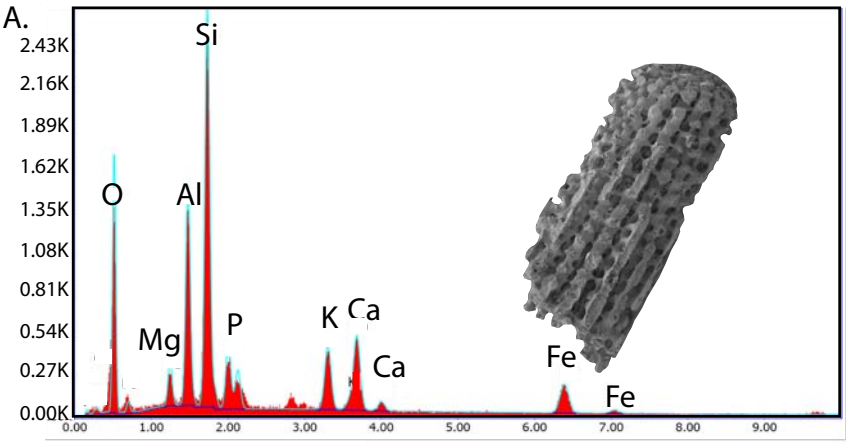
2.43K
2.16K
1.89K
1.62K
1.35K
1.08K
0.81K
0.54K
0.27K
0.00K
Si
O
Al
Mg
P
K
Ca
Ca
Fe
Fe
0.00
1.00
2.00
3.00
4.00
5.00
6.00
7.00
8.00
9.00

B.

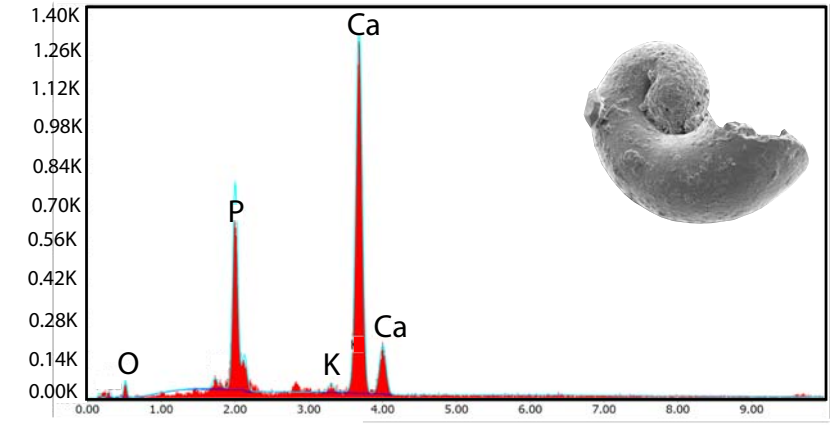
1.40K
1.26K
1.12K
0.98K
0.84K
0.70K
0.56K
0.42K
0.28K
0.14K
0.00K
Ca
P
Ca
O
K
0.00
1.00
2.00
3.00
4.00
5.00
6.00
7.00
8.00
9.00

C.

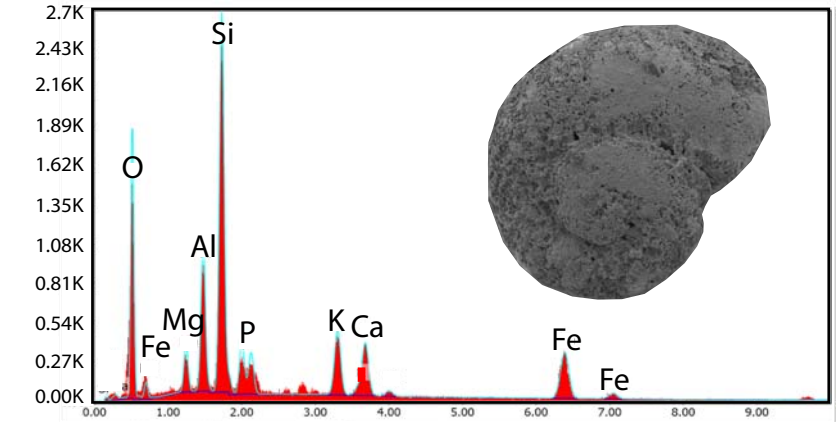
2.7K
2.43K
2.16K
1.89K
1.62K
1.35K
1.08K
0.81K
0.54K
0.27K
0.00K
Si
O
Al
Mg
Fe
P
K
Ca
Fe
Fe
0.00
1.00
2.00
3.00
4.00
5.00
6.00
7.00
8.00
9.00

D.

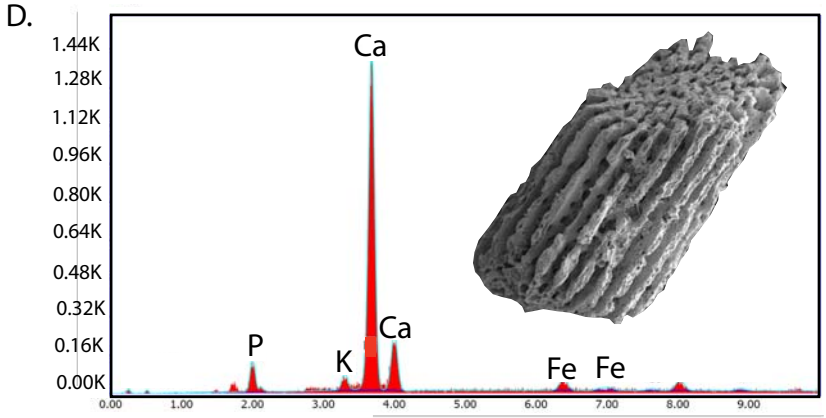
1.44K
1.28K
1.12K
0.96K
0.80K
0.64K
0.48K
0.32K
0.16K
0.00K
Ca
P
K
Ca
Fe
Fe
0.00
1.00
2.00
3.00
4.00
5.00
6.00
7.00
8.00
9.00

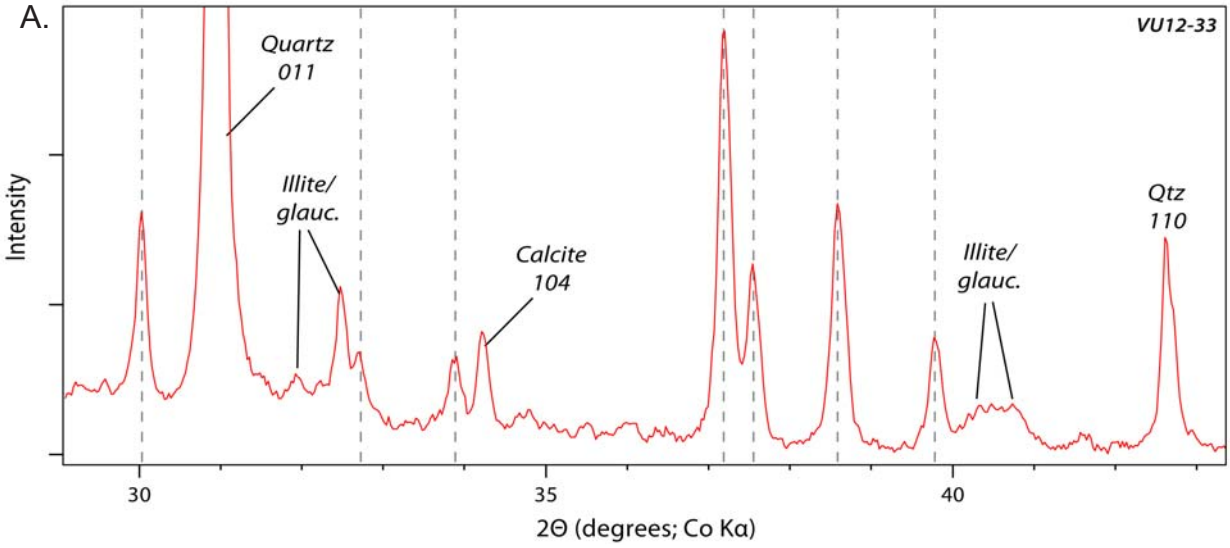
A.
VU12-33
Quartz
011
Illite/
glauc.
Calcite
104
Illite/
glauc.
Qtz
110
Intensity
30
35
40
2Θ (degrees; Co Kα)

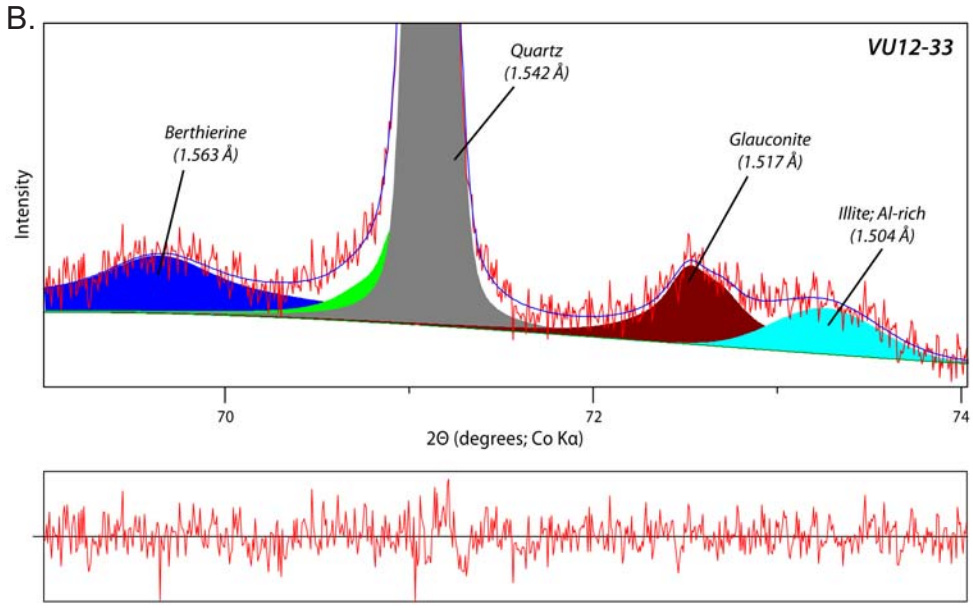
B.
VU12-33
Quartz
(1.542 Å)
Berthierine
(1.563 Å)
Glauconite
(1.517 Å)
Illite; Al-rich
(1.504 Å)
Intensity
70
72
74
2Θ (degrees; Co Kα)

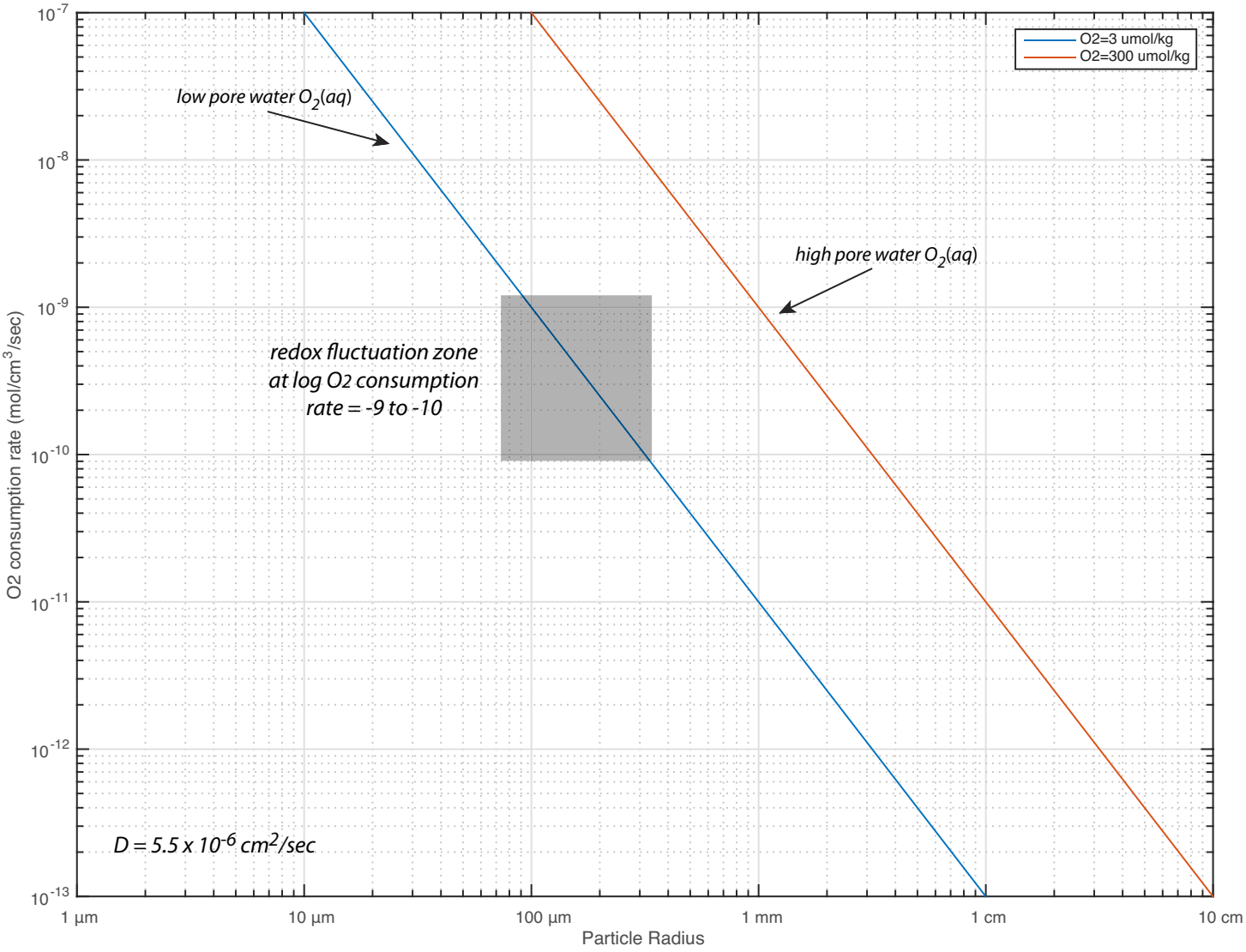
O2=3 umol/kg
O2=300 umol/kg
low pore water $O_2(aq)$
high pore water $O_2(aq)$
redox fluctuation zone
at log O2 consumption
rate = -9 to -10
$D = 5.5 \times 10^{-6}$ cm^2/sec
O2 consumption rate (mol/cm^3/sec)
10^{-7}
10^{-8}
10^{-9}
10^{-10}
10^{-11}
10^{-12}
10^{-13}
1 µm
10 µm
100 µm
1 mm
1 cm
10 cm
Particle Radius

TABLE 1. Mineral composition of fossiliferous residues from XRD (x-ray diffraction)

Sample	Quar	Calc	Dolo	Apat	Illite	Glauc	Kaol	Goet	Pyr	Plag	Berth
VU12-33	37	2		16	7	10	Tr			22	6
VMM12-38	83	1	5	4	5	1					
VMM12-42	90	1	1	4	Tr	1		3			
VMM16-46A	55	1			21	23		1			Tr
VMM12-46B	25		64	4	3	2			Tr		2
VMM16-48A	69	21		8	Tr	Tr	Tr	3			